Infrared Imaging of a Solid Phase Surfactant Monolayer

T. A. Conover and J. R. Saylor*

Department of Mechanical Engineering, Clemson University, Clemson, South Carolina 29634-0921

Received February 5, 2006. In Final Form: June 2, 2006

A new method for visualizing solid phase surfactant monolayers is presented. This method utilizes infrared (IR) imaging of the surface of a warm subphase covered by the monolayer. When the subphase is deep, natural convection occurs, resulting in a complex surface temperature field that is easily visualized using an IR camera. The presence of a surfactant monolayer changes the hydrodynamic boundary condition at the interface, dramatically altering the surface temperature field, and permitting the differentiation of surfactant-covered and surfactant-free regions. In this work, solid phase monolayers are imaged using this IR method. Fractures in the monolayer are dramatically visualized because of the sudden elimination of surfactant in the region opened up by the crack. The method is demonstrated in a wind/water tunnel, where a stearic acid monolayer is deposited and a crack is created through shear on the surfactant surface, created by suddenly increasing the velocity of the air over the water.

1. Introduction

Many optical methods exist for the study of surfactant monolayers. For example, the thickness of these surfactant films can be ascertained via ellipsometry and by interferometric methods.[1] Characteristics of the chemical composition and structure of surfactant monolayers can be obtained via various spectroscopic and fluorescence based measurements.[2] Images of surfactant monolayers have been obtained through a variety of methods including Brewster angle microscopy (BAM)[3] and ultramicroscopy,[1,2] both of which have been used to visualize the microstructure of solid-phase monolayers, revealing the existence of grain boundaries, defects and locations of monolayer collapse. Transfer of monolayers to a solid substrate (e.g., via the Langmuir−Blodgett technique) facilitates the use of a host of more modern methods such as atomic force microscopy (AFM),[4,5] scanning tunneling microscopy (STM),[4,5] auger electron spectroscopy (AES),[3] and X-ray photoelectron spectroscopy (XPS).[3]

An important reason for studying surfactant monolayers is their environmental relevance, namely how they mediate the transfer of heat, water, and dissolved gases across the air/water interfaces of lakes, oceans, and rivers. Much remains unknown about the role of monolayers in these situations, and the microscopic tools described above, as well as other laboratory techniques such as the Wilhelmy plate and the Langmuir trough, are of limited use on water surfaces of any sizable area. Hence a need exists for diagnostics that permit visualization of surfactant monolayers over broad regions of an air/water interface.

Infrared imagery presents a method by which surfactant monolayers can be studied over very small or very large areas. If a warm body of water transfers heat to the air above it, the surface of the water becomes cooler and its density increases, resulting in a buoyant instability that drives natural convection in the water. This can also occur when the air and the water are at the same temperature, but the air has a relative humidity less than 100%, wherein natural convection is driven by evaporative cooling at the water surface. The fluid motion caused by natural convection results in a complicated temperature field on the water surface that can be imaged with an IR camera. An example of such a temperature field is presented in Figure 1a. This image shows a temperature field of a warm body of water, ∼17 cm on a side, showing cool (dark) regions consisting of thin lines, interspersed with warm (light colored) regions. The cool thin lines are the surface manifestations of sheets that fall into the bulk while the warm bright regions are the surface manifestations of rising plumes.[7] It is clear that there is turbulent activity in the water at very small scales. When a water surface is surfactant-free, and there is no externally imposed air flow, as is the case in Figure 1a, a shear-free boundary condition exists at that surface. When a surface is surfactant-covered, however, a constant elasticity boundary condition exists. The presence of elasticity on a surfactant-covered interface damps the convective velocity fluctuations near that interface and thereby affects the surface temperature field. This can be seen in Figure 1b, which is an IR image of the surface of a water body having approximately the same heat flux, size, and depth as for Figure 1a, but has a monolayer of the liquid-phase surfactant, oleyl alcohol. The elimination of small scale variations in the surface temperature field caused by the surfactant, is easily seen. The dramatic difference between panels a and b in Figure 1 shows how IR imagery can effectively determine the presence of a surfactant.

Infrared imagery has been used to study various aspects of liquid-phase surfactant monolayers (including adventitious surfactants found in tap water). Saylor et al.[6,8] used infrared imaging to demonstrate the effect of liquid-phase surfactant monolayers on the statistics of the surface temperature field as well as how the heat flux emanating from an air/water interface affects the surface temperature field. Infrared imaging has been used to visualize spreading of an oleyl alcohol monolayer.[9] It has been shown that, in some cases, infrared imagery reveals the presence

* To whom correspondence should be addressed.

(1) Gaines Jr., G. L. *Insoluble Monolayers at Liquid−Gas Interfaces*; John Wiley & Sons: New York, 1966.

(2) Adamson, A. W. *Physical Chemistry of Surfaces*; John Wiley & Sons: New York, 1990.

(3) Petty, M. C. *Langmuir−Blodgett Films: An Introduction*; Cambridge University Press: Cambridge, MA, 1996.

(4) Birdi, K. S.; Vu, D. T. Application of scanning probe microscopy (scanning tunneling microscopy and atomic force microscopy) in colloid and surface chemistry. In *Handbook of Surface and Colloid Chemistry*; Birdi, K. S., Ed.; CRC Press: Boca Raton, FL, 2003.

(5) Lyklema, J. *Fundamentals of Interface and Colloid Science*. *Volume III*: *Liquid-Fluid Interfaces*; Academic Press: New York, 2000.

(6) Saylor, J. R.; Smith, G. B.; Flack, K. A. *Int. J. Heat Mass Transfer* **2000**, *43*, 3073−3086.

(7) Saylor, J. R.; Flack, K. A.; Schultz, M. P.; Smith, G. B. *Exp. Fluids* **2002**, *32*, 570−579.

(8) Saylor, J. R.; Smith, G. B.; Flack, K. A. *Phys. Fluids* **2001**, *13*, 428−439.

(9) Saylor, J. R.; Smith, G. B.; Flack, K. A. *Phys. Fluids* **2000**, *12*, 597−602.

10.1021/la060345g CCC: $33.50
Published on Web 07/06/2006

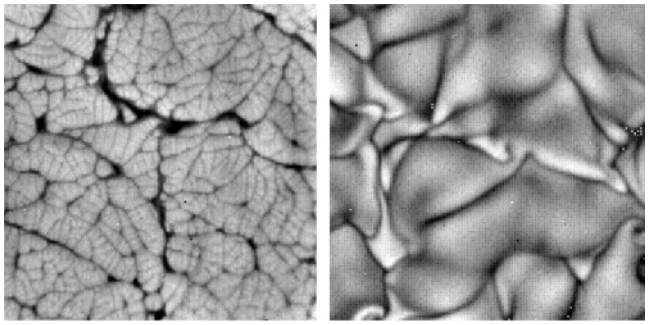

Figure 1. Comparison of the surface temperature field for two bodies of water at zero wind speed for the case of (a) clean surface conditions, and (b) a surfactant-covered condition. The heat flux is 407 W/m^2 in both cases. Warm regions are white and cooler regions are dark. The surfactant is oleyl alcohol having a surface concentration of 0.11 μg/cm^2 in (b). The size of the two images is 17.1 and 15.7 cm for (a) and (b), respectively. (Reprinted with permission from ref 6, Copyright 2000 by Elsevier.)

of surfactant monolayers when a Wilhelmy balance and Langmuir trough combination show no change in surface pressure.[10] Phongikaroon et al.[11] used infrared imaging to visualize the location of a Reynolds ridge defining the boundary between surfactant-covered and clean water in a wind/water tunnel, and Judd et al.[12] showed what appears to be a surfactant/clean water boundary when studying the impingement of an air jet onto a water surface, also using infrared imagery. Despite the above work, to the authors' knowledge, there has been no investigation of the use of infrared imagery to investigate solid-phase surfactant monolayers.

The surfactant films that are observed on lakes and oceans are a complex mixture of compounds that exhibit significant variations over space and time.[13] However, it is generally thought that these films, as variable as they are, are of the gaseous phase,[14] viz. not solid phase. However, in coastal regions where point and diffuse sources of pollution exist, surfactants of any phase may exist due to the diversity of chemicals that comprise water pollution. For example, many fatty acids and alcohols exhibit solid-phase surfactant behavior when their chain length is sufficiently long.[2] Such fatty acids (of which stearic acid is an example) are found in food industry effluents, for example,[15] demonstrating the relevance of solid-phase surfactants in coastal regions.

2. Experimental Section

A wind/water tunnel was used to study a monolayer of the solid-phase surfactant stearic acid. The monolayer was located on a warm water surface, and the air flow exerted a shear stress upon the monolayer. Figure 2 is a drawing of this facility, which consists of a tank of warm water which was filled to the rim, and a simple wind tunnel constructed to provide a flow of room-temperature air across the water surface. The internal dimensions of the tank are 1003 mm long (the wind direction) by 250 mm wide by 380 mm deep. The air flow generates a shear across the water surface, exerting a force

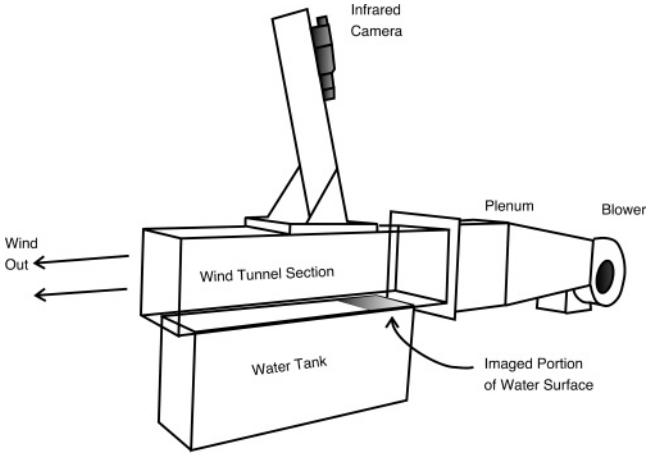

Figure 2. Line drawing of the experimental facility.

upon any surfactant at the air/water interface. As shown in the following section, this can fracture a sold phase surfactant, permitting visualization of this event.

The IR camera used here was a 252 × 238 pixel cooled CCD (Inframetrics ThermaCAM SC1000). The temperature resolution of IR cameras is quantified by the noise equivalent ΔT (NEDT), which is a measure of the noise level in terms of temperature. For this camera, the NEDT was 0.07 K. For comparison, the range in temperatures exhibited in Figure 1 is approximately 1 K. The camera was mounted at a 16° incidence angle so that it could not see its own reflection. The IR camera used in this work is sensitive to the wavelengths $\lambda = 3-5$ μm. The optical depth of water in this range of wavelengths is ~25 microns. Hence, the infrared images presented here are maps of the temperature averaged over the top 25 μm of water, essentially a surface temperature field. A frame grabber was used to capture the monochrome analog video output, which was stored on a personal computer in real time as uncompressed TIFF images. A hand-held anemometer was used to measure the speed of the air over the water surface, which was used to determine the wind speed at which the solid-phase monolayer fractured.

At the beginning of each experiment, the tank was filled with warm tap water. The water surface was skimmed to remove indigenous surfactants present on the surface. The surface was then covered with approximately 1 mL of a heptane/stearic acid solution, having a concentration of 1.4 mg/mL. The heptane evaporated from the surface of the water within several seconds, leaving a stearic acid monolayer having a surface concentration of approximately 0.6 μg/cm^2. At collapse pressure, the concentration of stearic acid is 0.23 μg/cm^2,[16] about 2.5 times less than the concentration used here. As will be noted below, the IR imagery obtained here showed several blemishes in the monolayer. These are most likely regions of monolayer collapse and multilayer regions, which would account for the difference between the concentration applied to the surface and the known collapse pressure. Other than the regions showing blemishes, we expect the monolayer to have a thickness approximately equal to the length of the stearic acid molecule; that is, we assume that the molecules are close-packed.[1] Blodgett[17] showed that a monolayer of stearic acid, deposited on a solid has a thickness of 24.4 Å, which she pointed out agreed well with published data for the length of the molecule, obtained by X-ray measurements of stearic acid crystals. [Due to the presence of Ca ions in the water subphase used to create these Langmuir−Blodgett films, the monolayers were actually calcium stearate, but these are not expected to be significantly different from stearic acid monolayers.] Hence we expect that the thickness of the stearic acid monolayers in this work is ~24.4 Å. Because the IR radiation collected by the camera is in the 3−5 μm wavelength band, the radiation being collected is approximately 1000 times larger than the monolayer thickness and therefore the monolayer is essentially transparent.

(10) Saylor, J. R. *Rev. Sci. Instrum.* **2001**, *72*, 4408−4414.
(11) Phongikaroon, S.; Judd, K. P.; Smith, G. B.; Handler, R. A. *Exp. Fluids* **2004**, *37*, 153−158.
(12) Judd, K. P.; Phongikaroon, S.; Smith, G. B.; Handler, R. A. *Exp. Fluids* **2005**, *38*, 99−111.
(13) Frew, N. M.; Nelson, R. K. *J. Geophys. Res.* **1992**, *97*, 5291−5300.
(14) Barger, W. R.; Means, J. C. Clues to the structure of marine organic material from the study of physical properties of surface films. In *Marine and Estuarine Geochemistry*; Sigleo, A. C., Hattori, A., Eds.; Lewis Publishing: Chelsea, MI, 1985.
(15) Renard, B.; Barbier Jr., J.; Duprez, D.; Durécu, S. *Appl. Catal. B* **2005**, *55*, 1−10.
(16) Kundu, S.; Datta, A.; Hazra, S. *Langmuir* **2005**, *21*, 5894−5900.
(17) Blodgett, K. B. *J. Am. Chem. Soc.* **1935**, *57*, 1007−1022.

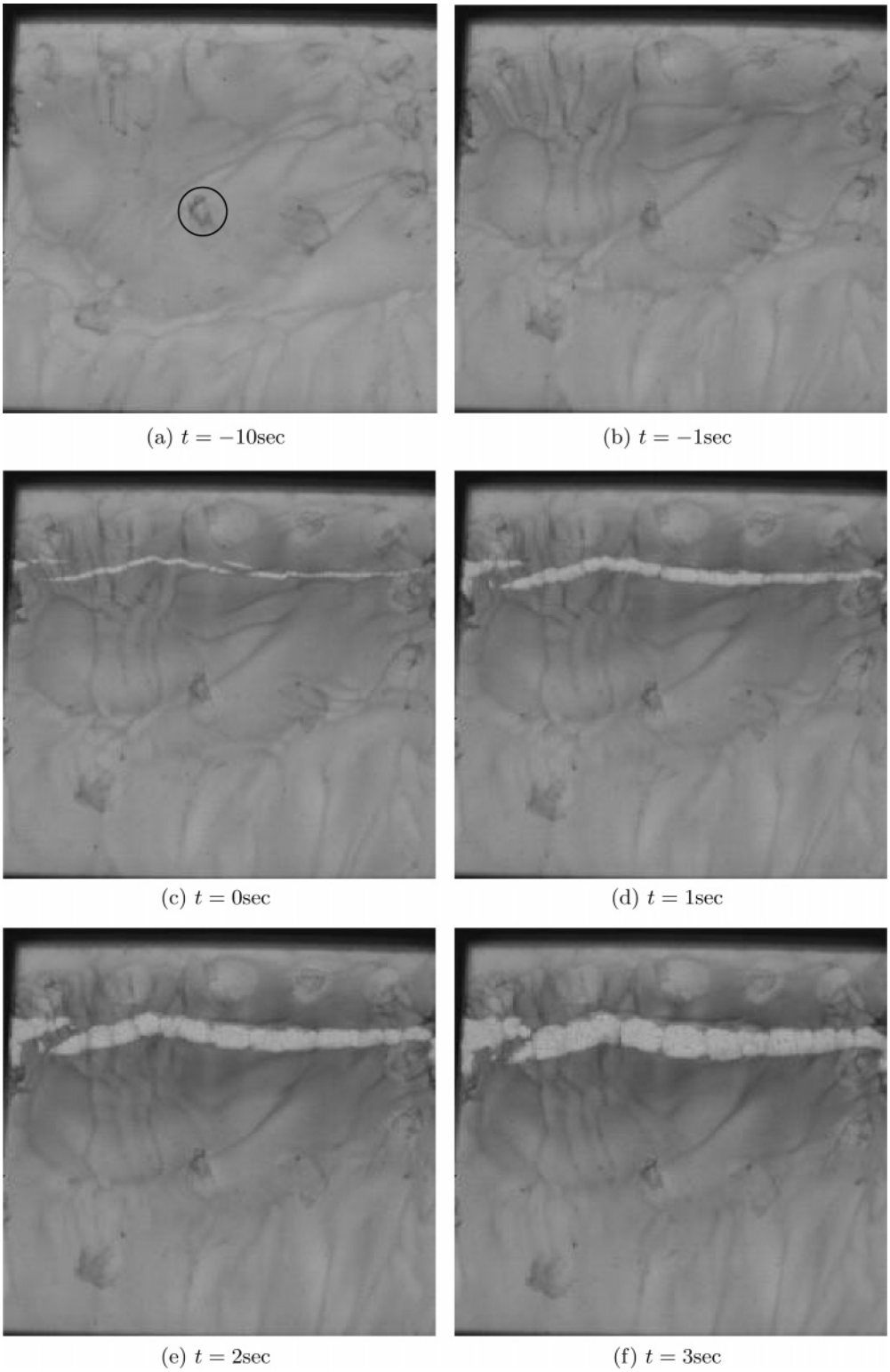

Figure 3. Sequence of infrared images revealing formation of a crack in the stearic acid monolayer. Stearic acid surface concentration ~0.6 μg/cm^2. Minimum gray level corresponds to 29.7 °C, and maximum gray level corresponds to 39.9 °C.

After the monolayer was created, the blower was turned on and set to a speed of 2.0 m/s and allowed to run for several minutes in order to establish a steady-state natural convection flow in the water beneath the monolayer. Allowing this period of time to pass permits the natural convection to involve the full depth of the tank. Because the solid phase surfactant does not move (prior to any fracturing event), the air serves solely to cool the air/water interface, viz. the air does not push the water surface downstream. Once steady state was achieved in the infrared imagery, the frame grabber was activated to capture video from the camera, and the wind speed was rapidly increased to 4.0 m/s. Fracture of the stearic acid monolayer was observed shortly thereafter.

3. Results and Discussion

Images are presented here from two experiments and are presented in Figures 3 and 4. In all of these images, the air flow is moving from top to bottom, and the upper boundary of the frame corresponds to the upstream edge of the tank. Each image is 25 cm × 25 cm in extent, and the spatial resolution is 0.99

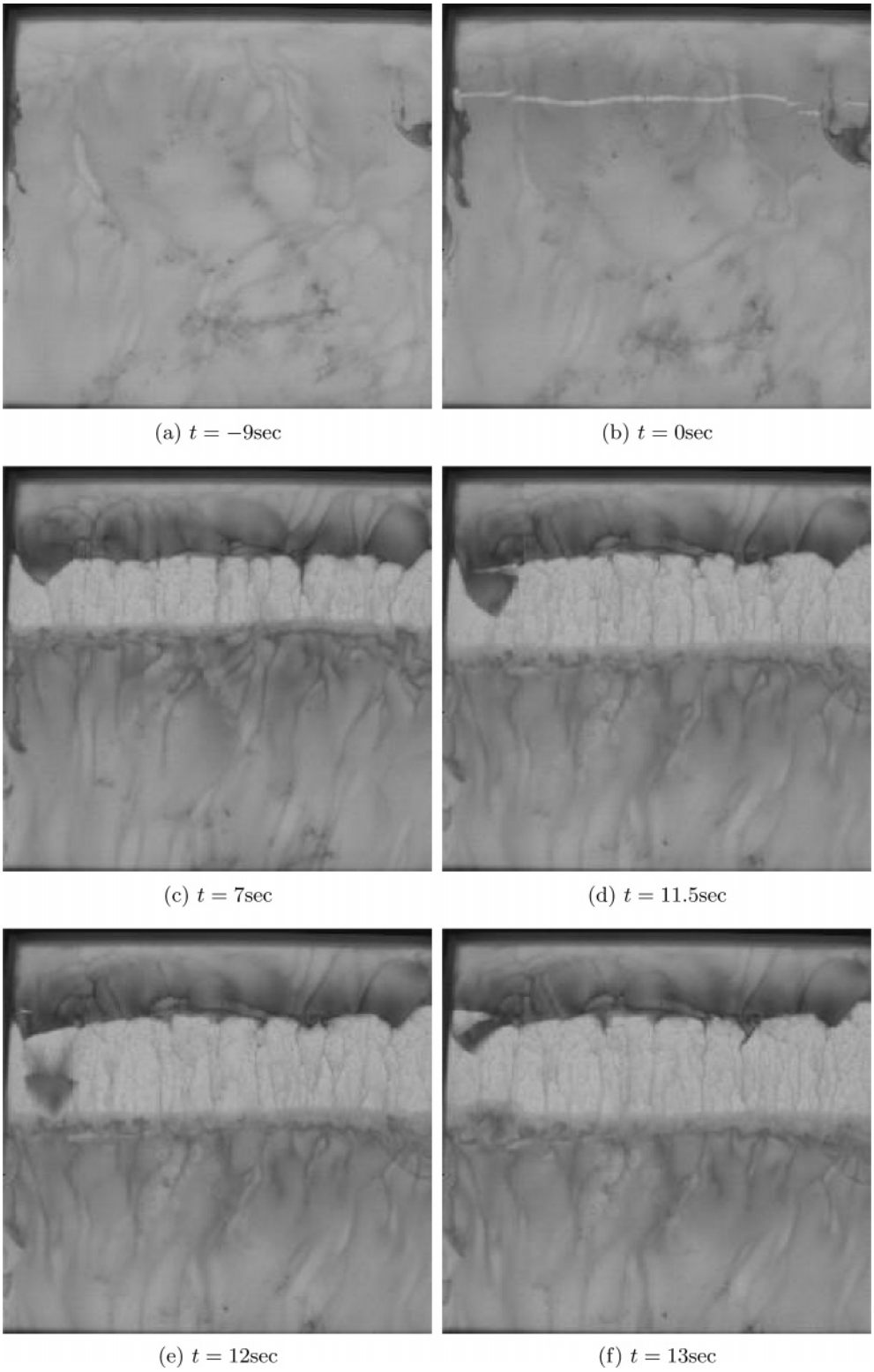

Figure 4. Sequence of infrared images showing a calving event in the solid-phase monolayer. The stearic acid surface concentration is ~0.6 μg/cm^2. Minimum gray level corresponds to 29.2 °C, and maximum gray level corresponds to 39.9 °C.

mm/pixel. Each frame in Figures 3 and 4 has a time annotation, with a datum of $t = 0$ which is the instant where a crack in the monolayer was first observed.

Prior to film fracture (Figure 3, panels a and b, for example), the air/water interface is being cooled by forced convection due to the flow of air over the solid monolayer; heat is transferred by conduction through this monolayer from the warm water to the cooler air. Because the monolayer is intact, solid, and unmoving, the air does not directly cause motion of the water via shear. Rather, by cooling via conduction through the surfactant film, natural convection is induced as water near the surface is cooled, becomes more dense, and sinks into the bulk. The regions where water is sinking are seen in the imagery as dark (cool), branching, curvilinear features which are the surface manifestations of cool sheets falling into the bulk, analogous to those seen in Figure 1. The relatively warmer fluid that replaces these falling sheets is seen as the broader, lighter gray regions between these sheets. Observing these images as a movie shows that these

structures move both upstream and downstream, demonstrating that the solid phase monolayer is indeed completely supporting the air shear. Note that (prior to fracture of the film) the similarity between the structures observed in Figures 3 and 4 and those observed in Figure 1b, which is for zero wind speed, is expected since the water in both cases is not experiencing a wind-induced shear.

The monomolecular nature of these surfactant films prevents their direct visualization; it is the alteration of the convective thermal patterns that is actually observed. A useful exception to this statement concerns the presence of blemishes in the monolayer, described in the previous section. The monolayers presented here were imperfectly formed and exhibit isolated blemishes in locations where lenses of heptane evaporated. These blemishes are easily seen in the images and may be regions of multilayers or monolayer collapse. An example of one is circled in Figure 3a. These blemishes are helpful in that they permit differentiation between the surfactant monolayer and changes in the thermal patterns of the water surface, as seen through the monolayer. For example, in Figure 3, panels a and b, the blemish identified by the circle is unmoved, whereas the curvilinear structures have moved significantly during the 9 s interval between the two images.

A crack in the monolayer is first seen in Figure 3c. The crack is seen as the horizontally oriented (cross-stream) region of much warmer fluid (white in these gray scale infrared images). This increase in temperature is due to the fact that the bulk fluid, which is warmer than that of the surface, is now free to move to the surface, unimpeded by the monolayer. Hence when the wind moves the monolayer downstream, the warm bulk water is exposed revealing a region in the IR image that is distinctly warmer than the surfactant-covered surroundings. Since the surfactant film has been fractured and moved, the region within the crack is presumed to be free of surfactants. The water used here was tap water, and eventually an indigenous monolayer comprised of organic contaminants in the tap water would form on the surface. However this would take some time and the imagery in the crack region is seen to resemble that of the clean case presented in Figure 1a. We note that when observed on video the monolayer can be seen to stretch slightly just before fracturing.

After the crack has formed, the portion of the monolayer downstream of the crack begins to move further downstream. Presumably there is a region of film collapse near the far downstream end of the tank, which crumples as the upstream portion of the surfactant film is transferred downstream. However this must be considered speculative since images were not acquired in these downstream regions. As the downstream portion of the surfactant film continues to move, as shown in Figure 3c−f, the streamwise dimension of the crack becomes larger. The sheetlike structures observed beneath the monolayer can also be seen in this surfactant-free region, but the length scale is much smaller. Also, these sheet structures in the surfactant-free region are oriented in the direction of the wind. This anisotropy is expected, since the water in this region is no longer protected from the wind by the solid-phase, stearic acid film.

In Figure 3, panels d and e, as the crack widens, a fragment of the monolayer is seen to break off and rotate counterclockwise slightly, revealing the solid-body rotation that is a characteristic of any solid object. In Figure 3f, the fragment separates from the upwind portion of the monolayer.

Figure 4 shows frames from the second experiment. A crack forms in a fashion similar to that shown in Figure 3. However, in Figure 4d, a portion of the upwind monolayer breaks off in a manner reminiscent of calving events observed on icebergs.[18] In Figure 4e, 12 s after fracture, the fragment has left the upstream portion of the monolayer but has not yet impacted the downstream portion. The fragment is less distinct in this frame, having warmed slightly while traversing the hot surface of the clean water. This is expected since, once the fragment separates, it moves with the wind. Hence, the velocity relative to the wind is smaller, and the rate of cooling for that piece of monolayer is concomitantly smaller, resulting in a temperature that is still cooler than the clean fluid, but not as cool as the nonmoving surfactant film. Also observed in Figure 4e are two cool trails that can be seen behind the fragment, making the fragment appear as if it has been stretched along the downstream direction. These presumably result from this relatively cool piece of monolayer cooling the local water region and leaving a slight trail in its wake as it travels downstream. An actual deformation has not occurred. At 13 s, the fragment is forced into the downwind portion of the stearic acid monolayer. At this moment, a second fragment is also seen separating from the upwind portion of the monolayer.

Finally, we note that in panels c−f in Figure 3, immediately after the crack forms, the temperature of the monolayer located on both the upwind and downwind side of the crack decreases, as evidenced by the horizontally oriented, diffuse, dark regions along the boundaries of the crack. It is unclear exactly why this occurs. When the monolayer fractures, the surface over which the air flows is no longer a uniform no-slip boundary condition. The exposed water surface is now moving with the wind, as is the downstream portion of the monolayer. This change in boundary condition will alter the air flow in the tunnel, and this may be responsible for the enhanced cooling on the upstream and downstream portion of the crack.

The above results show several ways in which IR imaging can be used in the study of surfactant monolayers. First, these results show that surfactant monolayers can be studied on a range of spatial scales. The images presented here were 25 cm on a side. However, they could just as easily be microscopic in nature to study buckling phenomena, for example. Alternatively, images such as those presented in this work may be obtained in the field from an aircraft platform[19−21] (for example) to investigate monolayers on lakes, over very large length scales. Hence, the possible range of length scales is large. Because the images presented here show dramatic differences between surfactant-covered and clean water surfaces, this method may provide a useful tool for ascertaining the presence or absence of monolayers in field studies of lakes and rivers. Second, since measurement of the velocity profiles in the air flow over the solid phase monolayer can be used to obtain the local shear stress, and from that the force exerted on the monolayer, it is possible that information regarding the intermolecular forces at the region of the fracture can be obtained. Several things prevent an accurate measure of the strength of the stearic acid monolayer that was fractured in this study. First, velocity profiles were not recorded, so precise measures of shear stress are not available. Second, because the stearic acid monolayer covered the entire water surface, the air shear served to simultaneously stretch the monolayer at the point of its attachment to the upstream wall and compress it in the downstream region. Hence, by definition, any computed monolayer strength would be an overestimate, since part of the shear was supported by monolayer compression in

(18) Joughin, I.; MacAyeal, D. R. *Geophys. Res. Lett.* **2005**, *32*, L02501.
(19) Marmorino, G. O.; Smith, G. B. *Geophys. Res. Lett.* **2005**, *32*, L11604.
(20) Marmorino, G. O.; Smith, G. B.; Lindemann, G. J. *Continental Shelf Res.* **2005**, *25*, 1−6.
(21) Marmorino, G. O.; Smith, G. B.; Lindemann, G. J. *Geophys. Res. Lett.* **2005**, *31*, L11309.

the downstream region. The above points notwithstanding, an order of magnitude estimate of the force required to fracture this monolayer can be obtained from empirical relations for shear stress, as will now be shown.

The flow of air over a solid surface is characterized by the Reynolds number

$$Re = \frac{u_\infty x}{\nu} \tag{1}$$

where u_∞ is the freestream velocity (the velocity far from the water surface), x is the downstream location, and ν is the kinematic viscosity of air. Choosing the midpoint along the tank length as an arbitrary analysis location, we find that $Re = 1.27 \times 10^5$, for $u_\infty = 4.0$ m/s, which exceeds the viscous stability limit for a laminar boundary layer, indicating that this flow is turbulent.[22] For turbulent boundary layers, the empirical relationship for the skin friction coefficient

$$\frac{c_f}{2} = \frac{0.0287}{Re_x^{0.2}} \tag{2}$$

may be used.[22] The skin friction coefficient is related to the wall shear stress via the equation

$$\tau_w = \frac{c_f}{2}\rho u_\infty^2 \tag{3}$$

giving a shear stress at the water surface of $\tau_w = 0.052$ N/m^2 for this case where $u_\infty = 4.0$ m/s, and $x = 0.5$ m. The average shear stress is

$$\overline{\tau_w} = \frac{1}{L}\int_0^L \tau_w(x)\, dx \tag{4}$$

where L is the tank length, 1.003 m, and τ_w is computed according to eq 3, giving $\overline{\tau_w} = 0.056$ N/m^2. Multiplying this average shear stress by the total surface area of the tank yields a characteristic force of 14 mN. This force can be compared to the collapse pressure of the monolayer. Collapse pressures are known to be a function of pH and ionic content of the subphase.[23] At a pH of 6.5 on pure water, the collapse pressure for stearic acid is $\Pi_c = 51$ mN/m (20.1 Å^2 area per molecule).[16] Multiplying Π_c by the tank width of 0.250 m, a characteristic collapse force of 12.75 mN is obtained, which is smaller than the characteristic force of the shear stress, computed above, by 1.25 mN. As noted earlier, the formation of a crack in this monolayer which completely covers the water surface requires compression (and ultimately collapse) of the monolayer in the downstream region and also separation (or fracture) in the upstream region. In theory, the force exerted by the wind shear on the monolayer in the region downstream of the crack must exceed both of these forces to form the crack. Hence, the difference between the characteristic shear force and the characteristic collapse force may be attributed to the attractive intermolecular forces between the stearic acid molecules. The above computation is rough in nature, and hence attributing the 1.25 mN difference to these forces is optimistic, especially since any forces due to attachment of the monolayer to the sidewalls has been ignored. More accurate values would be attainable should one obtain accurate velocity profiles so that the shear stress could be measured instead of estimated. An alternative way of performing this experiment would be to create a monolayer that did not extend to the downstream edge of the tank so that there would be no monolayer collapse pressure to overcome.

Further work is needed to determine how well suited this method is to field work. We have not presented any results here concerning the effect of ripples. With liquid phase surfactants, we have generally found that the IR field is modified surprisingly little when ripples are present, so long as they are not spilling or breaking. However, we have not investigated this for solid phase monolayers. Additionally, in the present work, the monolayer was initially attached to all four walls of the tank. This is unlikely to be the situation in a field environment, where solid-phase surfactants are more likely to be in the form of islands or films partially attached to the shore. It seems that the method should still be able to identify regions covered with a solid-phase surfactant, since the boundary condition will still be very different on the surfactant-covered region than the uncovered region. However, field experiments are needed to determine if this would be the case.

Acknowledgment. This work was supported by the U.S. Department of Energy under Contract No. DE-AC09-96SR18500.

LA060345G

(22) Kays, W. M.; Crawford, M. E.; Weigant, B. *Convective Heat and Mass Transfer*, 4th ed.; McGraw-Hill: New York, 2005.

(23) Binks, B. P. *Adv. Colloid Interface Sci.* **1991**, *34*, 343−432.